CORROSION SCIENCE AND TECHNOLOGY, Vol.20, No.3(2021), pp.118~128 pISSN 1598-6462 / eISSN 2288-6524
[Research Article] DOI: https://doi.org/10.14773/cst.2021.20.3.118

A way Analyzing Oxide Layer on an Irradiated CANDU-PHWR Pressure Tube Using an EPMA and X-ray Image Mapping

Yang Hong Jung† and Hee Moon Kim

Korea Atomic Energy Research Institute, 111- Daedeok-daero,989 Beon-gil, Yuseong-gu, Daejeon, 34057, Republic of Korea
(Received May 28, 2021; Revised June 09, 2021; Accepted June 09, 2021)

The oxide layer in samples taken from an irradiated Zr-2.5Nb pressure tube from a CANDU-PHWR reactor was analyzed using electron probe microanalysis (EPMA). The examined tube had been exposed to temperatures ranging from 264 to 306 °C and a neutron fluence of 8.9×10^{21} n/cm^2 (E > 1 MeV) for the maximum 10 effective full-power years in a nuclear power plant. Measuring oxide layer thickness generally employs optical microscopy. However, in this study, analysis of the oxide layer from the irradiated pressure tube components was undertaken through X-ray image mapping obtained using EPMA. The oxide layer characteristics were analyzed by X-ray image mapping with 256 × 256 pixels using EPMA. In addition, the slope of the oxide layer was measured for each location. A particular advantage of this study was that backscattered electrons and X-ray image mapping were obtained at a magnification of 9,000 when 20 kV volts and 30 uA of current were applied to radiation-shielded EPMA. The results of this study should usefully contribute to the study of the oxide layer properties of various types of metallic materials irradiated by high radiation in nuclear power plants.

Keywords: *Irradiated Zr-2.5Nb, CANDU-PHWR, Pressure tube, Oxide properties, EPMA*

1. Introduction

The oxidation reaction of Zr and its alloys takes place at the metal/oxide interface. Therefore, the oxidizing species should access the interface through the existing oxide layer in order to react with the metal and continue the oxidation process [1]. This fact should imply that the oxidation rate slows down with time, since the increasing diffusion path due to the growth of the oxide thickness causes a longer time for the oxidizing species to access the metal at the interface.

The oxidation of zirconium-based claddings has been studied extensively by many different methods worldwide with the strong impetus to improve the cladding corrosion performance for extended fuel burnups [2]. The corrosion properties of the alloys developed during the last 20 years are now satisfactory both for boiling water reactors (BWR) [3] and for pressurized water reactors (PWR) [4-6].

The oxidation process in nuclear power reactors is not easy to examine, since long irradiation cycles have to be awaited and in-pile measurements and probe techniques (even under test reactor conditions) are nearly not existent. In addition, results of post-irradiation tests of fuel pins are not always reproducible and in some situations, it is not possible to separate in an unambiguous manner material effects from hidden or obvious water chemistry changes.

Zr-2.5Nb pressure tubes are one of the main structural components in PHWRs that carry fuel bundles and heavy water of high temperature and high pressure inside them. Though their design life is predicted to be 30 years [7-9], it is yet to be demonstrated whether their integrity will be maintained even at the end of their life.

Inside the pressure tubes, heavy water coolant flows under a pressure of ~10 MPa and at a temperature of ~ 573 K. In earlier generation PHWRs, Zircaloy-2, an alloy of Zr with about 1.5% Sn, 0.20% Fe, 0.15% Cr, and 0.08% Ni, in cold-worked and stress-relieved (CWSR) condition, was used as pressure tube material [10,11]. During normal reactor operating condition, the flow of hot heavy water coolant through the pressure tubes causes slow oxidation of the inside surface of the tube, as represented by the chemical reaction:

$$Zr + 2D_2O = ZrO_2 + 4D \quad (1)$$

†Corresponding author: nyhjung@kaeri.re.kr
Yang Hong Jung: Principal Researcher, Hee Moon Kim: Principal Researcher

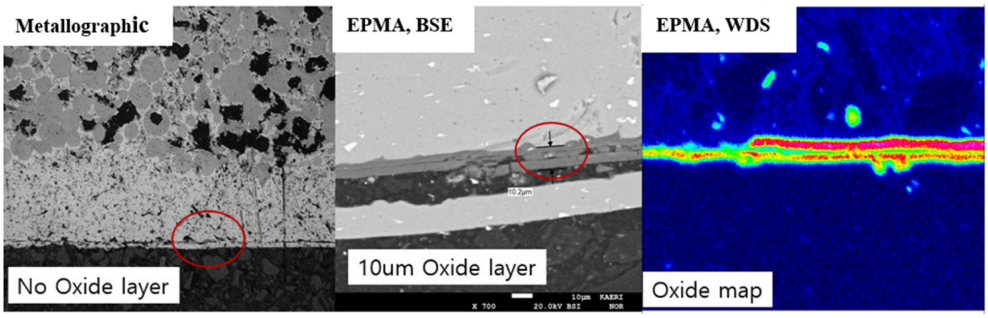

Fig. 1. Image of irradiated plate-type nuclear fuel by metallographic and EPMA BSE (× 700) and EPMA WDS oxide mapping

A part of hydrogen (H) or its isotope deuterium (D) produced in the above reaction is picked up by the pressure tube, causing hydride embrittlement [12]. The initial oxide layer formed on the surface is continuous, adherent, and impervious, and acts as a physical barrier against further oxidation. The Pilling-Bedworth ratio [13] of the oxide layer formed on zirconium metal is 1.56, which leads to the generation of compressive stresses in the oxide layer. As the oxide layer grows in thickness, the stress increases and becomes large enough to cause rupture of the oxide layer. Also, under the condition of high temperature, stress, and irradiation, the oxide layer is reported to recrystallize [14], resulting in micro-pore formation. It is reported [15] that once the oxide layer thickness exceeds 15 ~ 20 um, the oxidation rate is enhanced significantly as a consequence of micro-crack and micro-pore formation in the oxide.

The oxidized layer of the pressure tube irradiated in the CANDU-PHWR should be considered against existing studies examining the thickness or morphology of oxide layers using scanning electron microscopy. However, studies that have quantitatively analyzed the properties, profile, and chemical formula of oxide layers using an EPMA are scarce [12].

We attempted to determine the thickness of the oxide layer by analyzing irradiated plate-type nuclear fuel by metallographic as shown in Fig. 1. However, the oxide layer that I wanted to find could not be identified. Therefore, while considering various measures, we thought whether it would be possible to measure the thickness of the oxide layer using EPMA, and studied how the thickness of the oxide layer should be calculated if the oxide layer was identified using EPMA. We first attempted to analyze the oxide layer of Irradiated Zr-2.5Nb to measure the oxide layer thickness using the EPMA WDS Image mapping results. Since the thickness of the oxide layer, which was identified by metallographic, was acceptably accurate, we decided to calibrate the EPMA WDS Image mapping value based on this value.

In this study, the characteristics of CANDU-PHWR pressure tube oxide layers were measured using an electron probe micro analyzer and a X-ray mapping. And used as data to analyze the thickness of oxide layer using the unique value of the characteristic X-ray count of each pixel. This method may not have been attempted so far, or the results of the attempt may not be known. However, if the results obtained in this study are satisfactory, it can be usefully used for the analysis of the oxide layer of the Zr-2.5Nb pressure tube irradiated in the CANDU-PHWR reactor.

2. Experimental Preparations

2.1 Specimen preparation

The examined Zr-2.5Nb tube operated in a nuclear power plant for 10 effective full power years, reaching the maximum neutron fluence of 8.91×10^{21} n/cm^2 (E > 1 MeV). A tube ring of about 170 mm in length was taken from the middle of the tube. The average temperature and neutron fluence to which each tube ring was exposed ranged from 275.4 to 302.1 ºC and from 6.84×10^{21} to 8.91×10^{21} n/cm^2.

Specimens from the irradiated pressure tube were prepared in the hot cell facility at the Irradiated Material Examination Facility at Korea Atomic Energy Research Institute (KAERI), following the procedure developed for cutting small samples from an irradiated pressure tube piece. The procedure involved cutting a 5-mm-wide ring

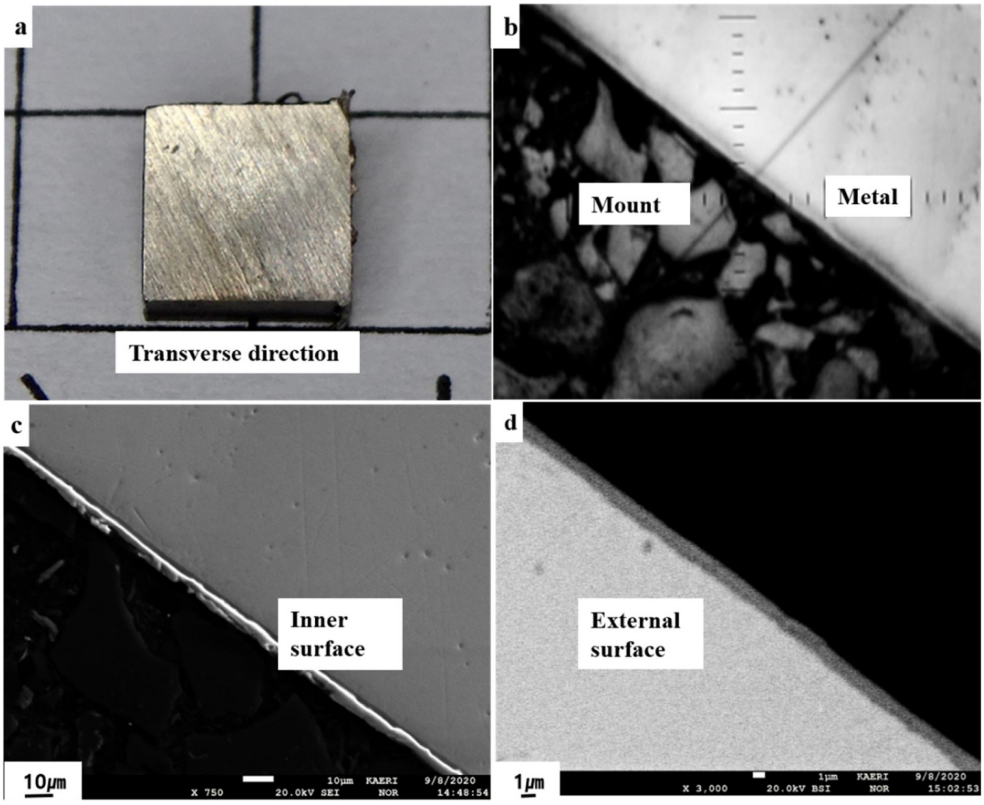

Fig. 2. Shape of irradiated Zr-2.5Nb pressure tube by camera (a), optical image (b, × 400), and BSE image of external surface (c) and SEM image of inner surface (d)

from the irradiated pressure tube using a remotely operated power saw inside a hot cell. Small samples for metallography and scanning electron microscopy (SEM) were then cut out from one of the pieces of the ring using a slow-speed cut-off machine. Samples were taken from the transverse direction, and as shown in Fig. 2a, the pressure tube specimen size is 6 mm × 5 mm × 4.2 mm (W × L × T). The radiation dose to the specimen was 330 uSv/hour. The specimen was ground and polished using a standard metallographic procedure. The examination of the oxide layer and measurement of its thickness was carried out on a polished surface of the sample.

2.2 Electron probe micro analyzer (EPMA)

The radiation shielded EPMA (JEOL JXA-8230R) used in this study was fabricated to be able to conduct an examination of highly irradiated fuels. In order to reduce the influence of radioactivity on a specimen's mounting area as well as the wavelength dispersive spectrometry (WDS) and column, the relevant parts were shielded with lead and tungsten. In addition, the specimen was cleaned with acetone in an ultrasonic cleaner to remove loose contaminations, and hot mounting was conducted in a hot cell with conductive resin. For the specimen, 20 kV and 30 nA were used. As a method to obtain X-ray image mapping for an oxide layer, analysis was performed for more than 6 hours to achieve satisfactory results.

As a method for X-ray image mapping with a magnification of 9,000, we used a beam scan mode, which is a method for scanning only an ion beam while the sample stage is fixed. The beam scan mode has the disadvantage of poor resolution when the incident current is too high, but satisfactory results can be obtained by inserting the current into the sample surface for a sufficient amount of time with the shape of the incident beam adjusted to optimal condition.

3. Results and Discussion

3.1 Oxide layer thickness by optical microscopy analysis

The method of measuring the thickness of the oxide layer generally uses optical microscopy analysis, as shown

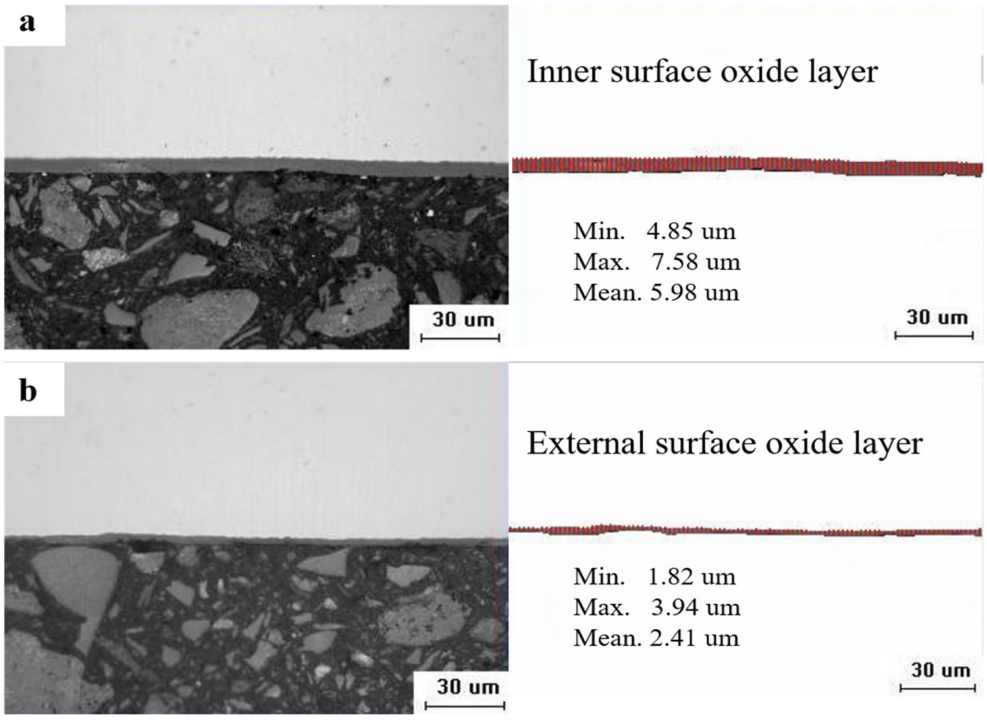

Fig. 3. Oxide layer thickness measured with optical microscopy (LEICA, Teletom-III) analysis, inner surface oxide layer (a), and external surface oxide layer(b)

in Fig. 3. In this study, the components of the oxide layer were closely monitored, and the chemical formula of the oxide layer was derived through the X-ray image mapping obtained using the EPMA based on the oxide layer thickness shown in Fig. 3.

Fig. 2 shows the preparation of the specimen. As already mentioned, this sample was cut in the transverse direction and prepared, as shown in Fig. 2, according to the sample preparation process. Fig. 2b shows an optical image mounted on an EPMA captured at a magnification of 400. As shown in the figure, the process of additional carbon deposition was not attempted because of the use of electrically conductive mount material. Fig. 2c shows a SEM image of the oxide layer on the inner surface of the sample. In addition, Fig. 2d shows a backscattered electron (BSE) image of the oxide layer on the outer surface of the sample, The reason why the BSE image was taken is because the oxide layer is very thin, so the oxide layer cannot be clearly seen by SEM. The oxide layer is roughly similar in thickness and the surface is not smooth, as shown in Fig. 2c. Fig. 3 shows the analysis results of optical microscopy (LEICA, Teletom-III) for the length of about 300 um. Fig. 3a shows the results for the oxide layer of the inner surface region. As shown in the figure, the overall thickness is relatively uniform, and the overall mean thickness is about 6 um. In contrast, Fig. 3b shows the thickness of the oxide layer in the external surface region, but the classification of the oxide layer is ambiguous in the image. It can be seen that the overall mean thickness is about 2.4 um. Based on this result, we can compare it with the X-ray image mapping analysis result.

3.2 Oxidation layer properties

X-ray image mapping data obtained using an EPMA are usefully used in various fields, including in analyzing traces elements of spent nuclear fuel. X-ray image mapping, which is mainly used in the analysis of various metal debris generated by the nuclear industry, has been used to identify the overall tendency of a particular element, as shown in Figs. 4 and 5. In this study, we derived a plan for how X-ray image mapping data can be used in the analysis of oxidation layer properties of a PHWR pressure tube. However, it was difficult to find reference data that has analyzed the oxide layer of a PHWR pressure tube by X-ray image mapping.

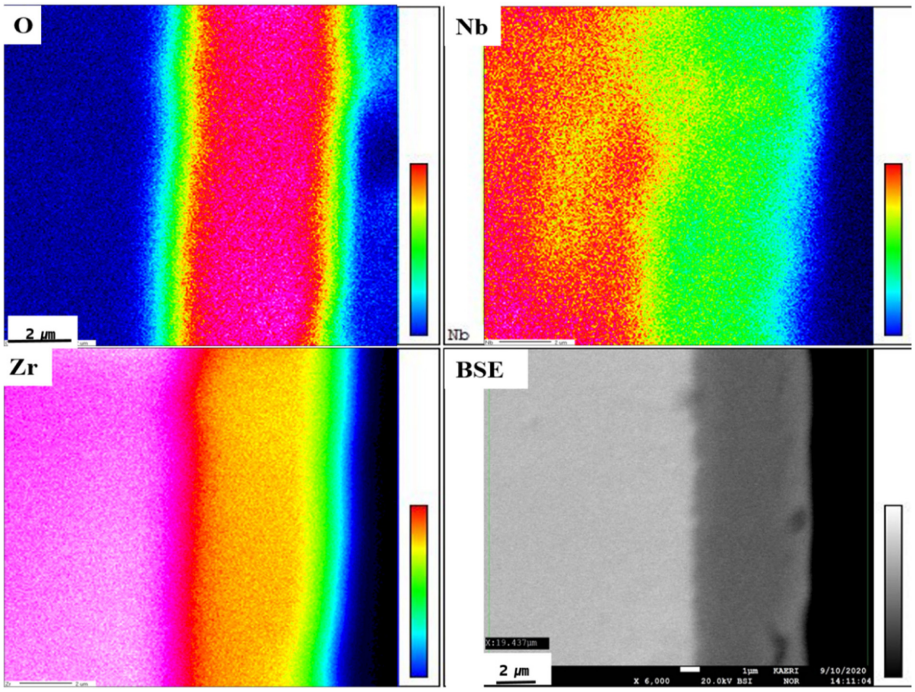

Fig. 4. X-ray image mapping of O, Nb, Zr and BSE image of internal surface (× 6,000)

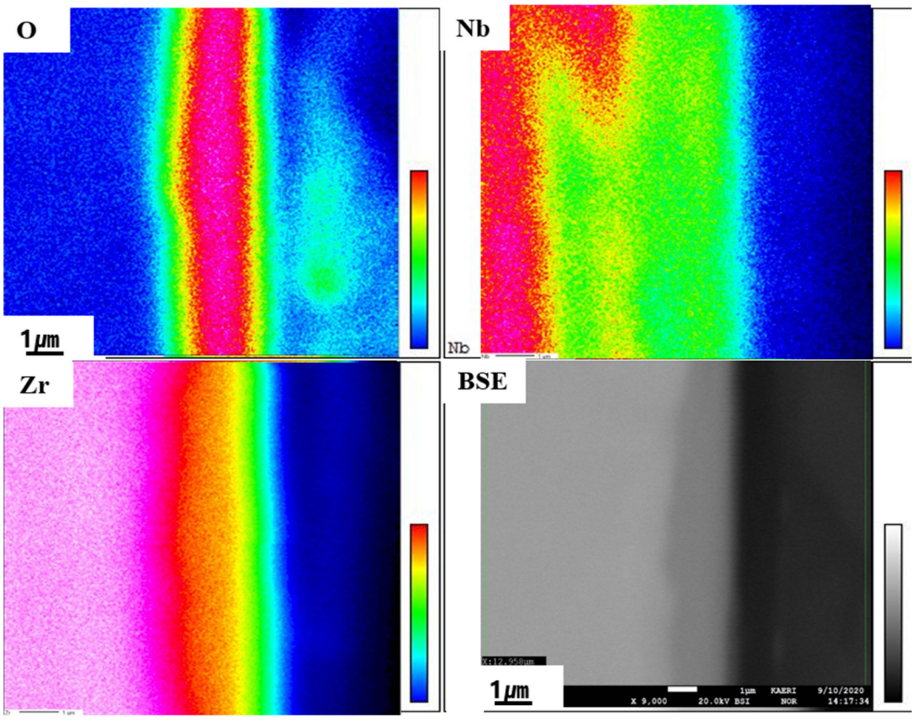

Fig. 5. X-ray image mapping of O, Nb, Zr and BSE image of external surface (× 9,000)

Fig. 4 shows the analysis results of the internal oxide layer obtained with the 15 um × 15 um area as 256 × 256 pixels, and Fig. 5 shows the external oxide layer acquired with the 10 um × 10 um area as 256 × 256 pixels. Using a shielded EPMA, as shown in Fig. 5, it is difficult to achieve the same results as shown 9,000 times the scale. In order to

achieve such a result, it was necessary to provide sufficient analysis time in the beam mode for at least 6 hours while stabilizing the ion beam and calibrating the beam size to achieve good results. Looking at these results in Fig. 4, the oxygen layer maintains a relatively constant composition, but it is judged that the thickness between the metal and the oxide layer and the thickness of the oxide layer and the resin region are likely to have almost the same value.

This phenomenon applies equally to the oxidation layer results in Fig. 5. First, we doubted that the ion beam size, which was adjusted to 1 um size, was due to the beam overlapping between the oxide layer and the metal. However, by comparing Fig. 4 analyzed at a magnification of 6,000 times and Fig. 5 analyzed at a magnification of 9,000 times, it could be confirmed that the result was not caused by beam overlapping. It was confirmed that these were equally functional in the Zr results in Figs. 4 and 5. The oxygen analysis in Fig. 4 shows that the vertical line is not clear and has a slight slope. To confirm this, the results of the analysis by dividing Fig. 4 into three parts and the results of the overall analysis were compared. As a result, the slope was not considered because it was within 2σ, which is an acceptable error range. Fig. 4 shows the results of the X-ray image mapping analysis of the oxide layer area of 15 um × 15 um with 256 × 256 pixels, and the method to achieve this is described as follows.

The characteristic X-ray emitted from the specimen was acquired 256 times and stored by scanning the electron beam with a diameter of 1 um in the fixed sample stage in the left and right directions of the specimen. In this way, 256 data were acquired in the vertical direction, and characteristic X-rays were acquired for a total of 65,536 pixles. By converting the stored characteristic X-ray value into Excel data, it can be used as the data shown in Fig. 6.

Based on the results of the oxygen X-ray image mapping analysis in Figs. 4 and 5, Fig. 6 shows the average data of 65,536 pixels of characteristic X-rays that analyzed the internal and external oxide layers of the specimen. First, looking at the internal oxide layer in Fig. 6, an area of about 8.5 um is related to the oxide layer out of the 15 um × 15 um region in total length. In the Figure, the inter-reaction region between the metal and the oxide layer occupies 37 pixels, which corresponds to 2.2 um in length (15 um / 256 × 37 pixels = 2.17 um). Here, the boundary divided into 37 pixels is at the no. 95 pixel point with a value of 68 cps, and the no. 133 pixel point, which is the 238 cps point (which is the 2σ value), is 95 percent of the oxide layer's average value of 250 cps.

Similarly, the interaction area of the oxide film and resin accounts for 35 pixels, which corresponds to 2.05 um in length (15 um / 256 × 35 pixels = 2.17 um). The boundary of the 35 pixels of the marking was calculated in the same way. From 205 pixels, 35 pixels were designated, which is a 2 σ value of 250 cps (the mean value of the oxide layer), up to the 239-pixel point with a value of 68 cps. Its slope is around 3.3, as shown in Fig. 6. The thickness of the oxide layer calculated by this method will refer to the value of 5.98 um shown in Fig. 3. As already mentioned, the ion beam size was 1 um. Assuming two distinct types of pure metals are in contact, at least 1 um distance beam overlapping will occur at their boundaries. Assuming that beam overlapping occurred in the boundary areas of the oxide layer front and rear side, 2.2 um and 2.1 um, in the Fig. 6, 1 um of each distance was estimated to be the oxide layer. Thus, the thickness of the oxide layer could be expressed as 6.3 um, as shown. It was confirmed that the values shown in Fig. 3 have similar values. Also, it could be confirmed that there is more than 1 um of interaction area at the boundary between the base metal and the oxide layer.

In the same way, based on the results of the oxygen X-ray image mapping analysis in Fig. 5, Fig. 6 shows the characteristics of the external oxide layer of the specimen. Looking at the outer oxide layer in Fig. 6, 3.5 um of the total length of the 10 um × 10 um region is related to the oxide layer. In the figure, the values for the inter-reaction zone between the metal and the oxide layer and the oxide layer and the resin were calculated in the same way as for the inner oxide layer. To determine the thickness of the oxide layer in the image created in this way, we refer to the value shown in Fig. 3, 2.4 um.

Something of particular note is the beam overlapping in the inner oxide layer. In the inner oxide layer, the ion beam size was clearly 1 um, and it was judged that beam overlapping occurred in the boundary region between the front and the rear side of the oxide layer, and 1 um was added to the thickness of the oxide layer, respectively.

However, as shown in Fig. 6, the values of the boundary area between the front and the rear side of the oxide layer are 1.4 um and 1.2 um. It is difficult to judge from the

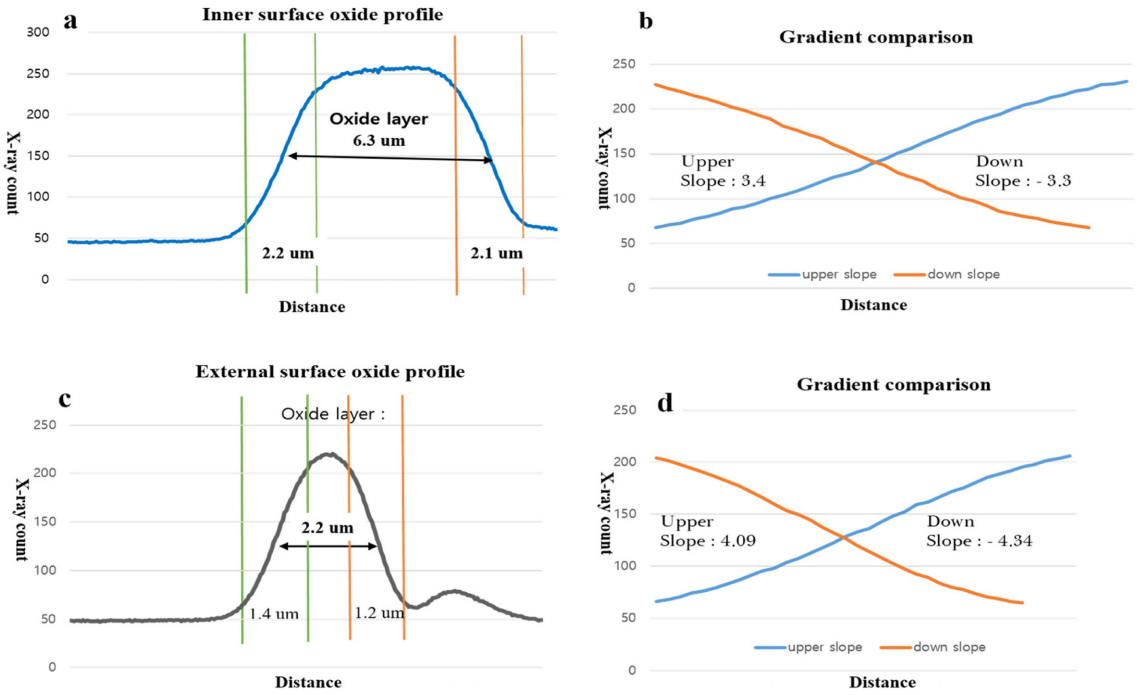

Fig. 6. Inner surface and external surface oxide profile and gradient comparison calculated by 256 × 256 pixels using an X-ray count

figure whether the values of the boundary regions are all generated by beam overlapping. Thus, we looked at the 142 cps area, which is the intersection of the slopes shown in Fig. 6b. In Fig. 6a, it was confirmed that the value of the oxide layer represented by the calculation formula was 6.3 um by the half value of the boundary area at the front and rear side of the oxide layer. As such, the slope crossing value in Fig. 6d was calculated by calculating 2.2 um, as shown in the figure, based on the 126 cps value. In the end, it was noted that when the distance between the front and the rear side of the oxide layer was divided by half and the distance of the pure oxide layer was added, a value similar to that of Fig. 3 was obtained.

Then, in Fig. 6c, we have no choice how the ion beam overlapping should be explained. In this case, assuming that the ion beam overlapping was performed over the entire oxide layer, after dividing 0.9 um, which is the distance of the pure oxide layer calculated at 256 pixels, by half, the front side value is 1.4 + 0.45 = 1.85, and the rear side value of 1.2 + 0.45 = 1.65 um is calculated. In other words, assuming the distance of the oxide layer is divided by half as the whole ion beam overlapping area, 1.85 + 1.65 = 3.5 um is calculated in Fig. 6c. If 2 um (the beam size of the front and the rear) is subtracted, the pure oxide layer area is 1.5 um. Although this value is different from the 2.4 um value shown in Fig. 3b, it can be confirmed that it is close to the image mapping value of oxygen shown in Fig. 5. That is, ion beam overlapping can explain X-ray image mapping with this calculation formula. Thus, the distance of the pure oxide layer obtained by X-ray image mapping can be measured with a calculated value calculated at 256 pixels.

As shown schematically in Fig. 6a, c, the slope shown in Fig. 6b, d shows that the inter-reaction boundary area of the outer oxide layer of the specimen is steeper than that of the inner side. This is the basis for judging that oxygen diffusion may have been slower on the outside than on the inside.

Fig. 7 shows a pictorial representation of data obtained with 256 × 256 pixels for the zirconium element. It can be seen that the profile of zirconium has a similar boundary area to that of oxygen. As shown in Fig. 7b, d, the slope of the boundary region between the metal and the oxide is smoother than that of the outermost boundary region between the oxide and the resin. However, the slope of oxygen shown in Fig. 6 is very low compared with that of zirconium, and the slope of the boundary regions on both sides of the oxide layer is almost the same.

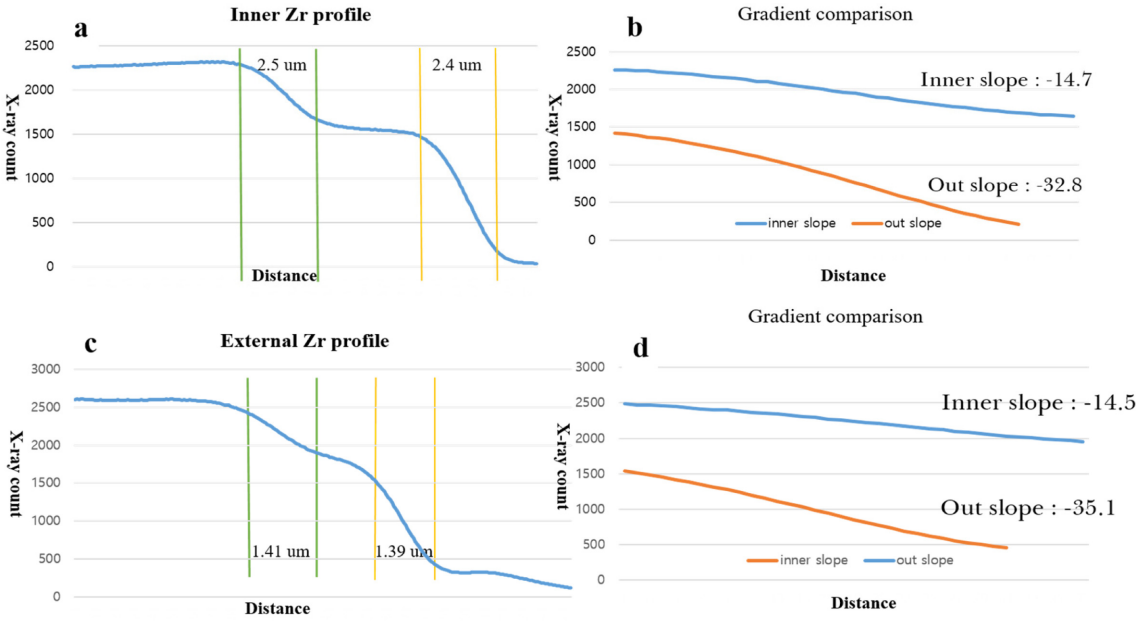

Fig. 7. Inner surface and external surface zirconium profile and gradient comparison calculated by 256×256 pixels using an X-ray count

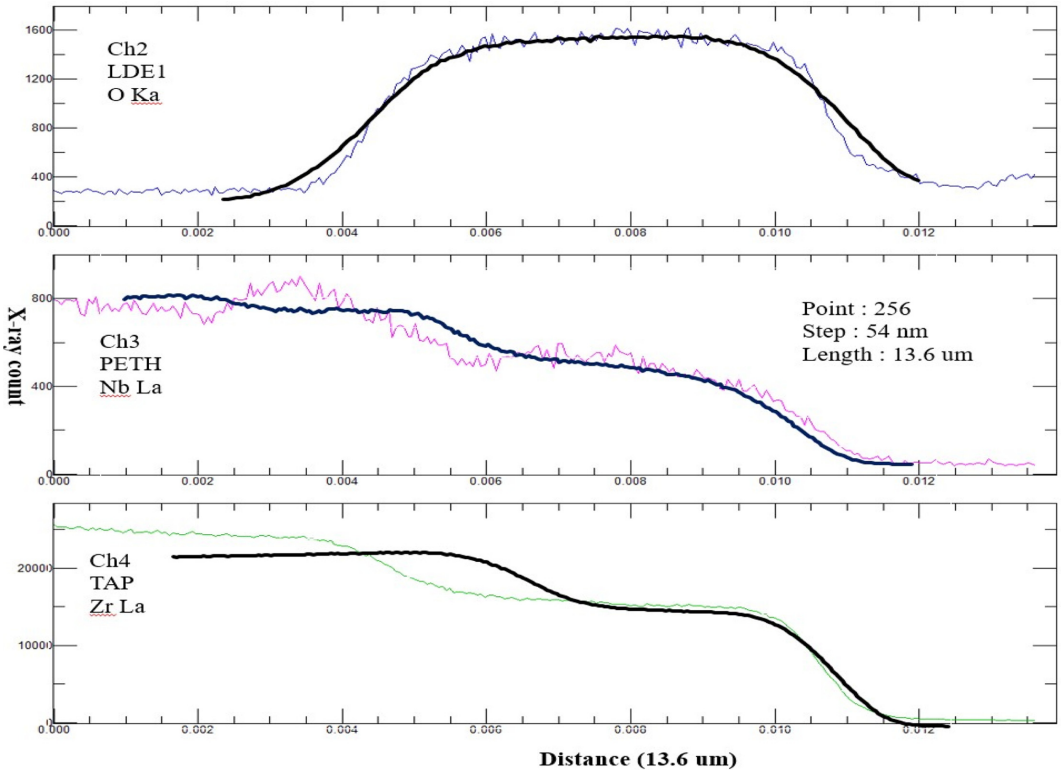

Fig. 8. Comparison of inner surface gradient by 256×256 pixels using an X-ray count (bold line) and single line Wavelength dispersive spectrometry analysis (thin line)

A low slope means easy movement, that is, the diffusion of elements with a low slope between the two elements reflects easy movement. Based on the slope of oxygen and zirconium, it can be seen that the diffusion of oxygen

is easier than that of zirconium. This means that this is not substitutional diffusion, but interstitial diffusion, and corresponds to N-type corrosion [16].

Fig. 8 shows the comparison of inner surface gradient by 256 × 256 pixels using X-ray count and single line WDS analysis. However, it was confirmed that the slope at both ends of the oxide layer showed some difference. In this figure, the use X-ray count and single line WDS analysis indicates that the thickness of the oxide layer is approximately determined when measuring the oxide layer with WDS. But it should be noted that Nb and Zr appear different enough to be considered. That is, when performing line analysis using WDS, it was confirmed that at least one line analysis did not reflect the element's representativeness.

3.2 Quantitative analysis using an EPMA

As mentioned previously, since the ion beam size was 1 um, the analysis distance of the sample was designated as at least 1 um to prevent beam overlapping. Table 1 shows the results of quantitative component analysis that summarized the average values of 5 neighboring points measured at a total thickness of 12 um on the inner side of the specimen. The distance between each analysis point is 1 um, so the data was measured at a total distance of 12 um. In this table, points 3, 4, and 5 are the boundary positions between the metal and the oxide film, which are well shown in Fig.s 6 and 7. As shown in this table, it can be seen that the ratio of oxygen to Zr is 2, and if it is expressed as a chemical formula, it is ZrO_2.

As shown in Table 1 above, the ratio of oxygen to Zr on the inner surface of the specimen was 2.02, which was about 2, but according to the results at point 4 measured on an external surface with a thickness of about 6 um as in Table 2, the ratio of oxygen to Zr is 2.16.

As such, it is estimated that the oxide on the inner

Table 1. Quantitative analysis results of an inner surface with in 12 um and its chemical formula from 5 to 10 analysis points

No.	O	Nb	Zr	Ratio (O/Zr)
1	12.76	2.42	84.81	0.2
2	7.77	2.23	90.00	0.1
3	14.26	2.49	83.25	0.2
4	38.59	1.22	60.19	0.6
5	63.38	0.92	35	1.81
6	64.98	0.80	34.25	1.90
7	66.65	0.77	32.59	2.05
8	67.08	0.57	32.35	2.07
9	67.9	0.48	32.61	2.08
10	68.27	0.67	31.06	2.20
11	69.7	0.32	29.98	4.3
12	71.82	0.28	9.90	9.1

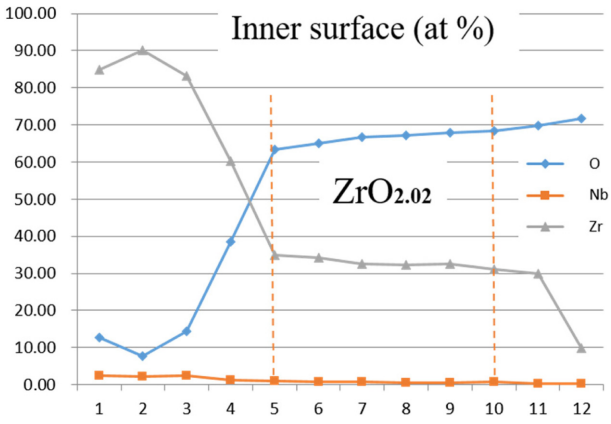

Table 2. Quantitative analysis results of the external surface with in 6 um and its chemical formula of point no. 4

No.	O	Nb	Zr	Ratio (O/Zr)
1	14.77	3.12	82.11	0.2
2	15.41	2.43	82.16	0.2
3	59.29	0.94	39.77	1.5
4	67.79	0.89	31.32	2.16
5	52.12	1.68	46.19	1.1
6	73.5	0.67	25.83	2.8

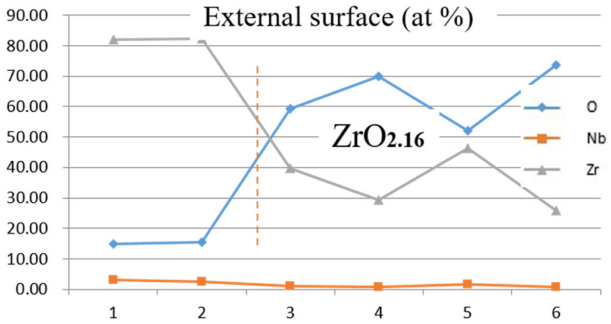

surface of the specimen is ZrO_2, while the oxide on the external surface is $ZrO_{2.16}$.

4. Conclusions

Samples taken from an irradiated Zr-2.5Nb pressure tube operating in a CANDU-PHWR reactor were examined using an electron probe micro analyzer (EPMA). Based on the results of the oxygen X-ray image mapping analysis, the thickness of the inner surface of the oxide layer could be expressed as 6.3 um. It was confirmed that the values by optical analysis have similar values. In addition, it was confirmed that there is more than 1 um of interaction area at the boundary between the base metal and the oxide layer. Quantitative analysis was performed on an inner and external surface of 12 um and 6 um length, respectively. The chemical formula of the oxide layer derived from this study was shown to be $ZrO_{2.02}$ and $ZrO_{2.16}$.

Based on the experimental method and concept attempted in this study, the method for analyzing oxide layers using an EPMA and its usefulness will be proven through additional experiments to establish a method for analyzing the oxide layer.

References

1. A. Grandjean and Y. Serruys, Metal and oxygen mobilities during Zircaloy-4 oxidation at high temperature, *Journal of Nuclear Materials*, **273**, 111 (1999). https://doi.org/10.1016/S0022-3115(99)00036-7
2. J. P. West, et al., Challenges for the Nuclear Fuel – A Utility Perspective in Light-Water-Reactor-Fuel-Performance, Park City Utah, ANS, Illinois, USA (2000).
3. G. Ledergerber, S. Abolhassani, M. Limbäck, R. J. Lundmark, and K.-Å. Magnusson, Characterization of high burnup fuel for safety related fuel testing, *Journal of Nuclear Science and Technology*, **43**, 1006 (2006). Doi: https://doi.org/10.1080/18811248.2006.9711189
4. J. Arborelius, M. Dahlbäck, L. Hallstadius, P. Jourdain, T. Andersson, R. Lisdat, M. Hahn, and E. Toscano, The Effect of Duplex Cladding Outer Component Tin Content on Corrosion, Hydrogen Pick-up, and Hydride Distribution at Very High Burnup, *Journal of ASTM International*, **2**, 1 (2005). Doi: https://doi.org/10.1520/JAI12411
5. IAEA (Ed.), Waterside Corrosion of Zirconium Alloys in Nuclear Power Plants, IAEA-TECDOC No. 996, IAEA, Vienna (1998). https://www.iaea.org/publications/5651/waterside-corrosion-of-zirconium-alloys-in-nuclear-power-plants
6. IAEA (Ed.), Corrosion of Zirconium Alloys in Nuclear Power Plants, IAEA-TECDOC-684, IAEA, Vienna (1993). https://www.iaea.org/publications/946/corrosion-of-zirconium-alloys-in-nuclear-power-plants
7. Final Safety Analysis Report of the Wolsong Unit-1 Nuclear Power Plant, Chapter 5, Korea Electric Power Company (1982).
8. M. K. Kumar, S. Aggarwal, V. Kain, T. Saario, and M. Bojinov, Effect of Dissolved Oxygen on Oxidation and Hydrogen Pick up behaviour-Zircaloy vs Zr-Nb alloys, *Nuclear Engineering and Design*, **240**, 985 (2010). Doi: https://doi.org/10.1016/j.nucengdes.2009.12.021
9. M. K. Kumar, I. Samajdar, N. Venkataramani, G. K. Dey, R. Tewari, D. Srivastava, and S. Banerjee, Explaining absence of texture development in cold rolled two-phase Zr–2.5 wt% Nb alloy, *Acta Materialia*, **51**, 625 (2003). Doi: https://doi.org/10.1016/S1359-6454(02)00442-1
10. D. Srivatsava, G. K. Dey, and S. Banerjee, Evolution of microstructure during fabrication of Zr-2.5 Wt pct Nb alloy pressure tubes, *Metallurgical and Materials Transactions A*, **26**, 2707 (1995). Doi: https://doi.org/10.1007/BF02669427
11. M. K. Kumar, C. Vanitha, I. Samajdar, G. K. Dey, R. Tewari, D. Srivastava, and S. Banerjee, Textural and Microstructural Developments during Fabrication of Zre2.5Nb Pressure Tubes, *Journal of Nuclear Materials*, **335**, 48 (2004). Doi: https://doi.org/10.1016/j.jnucmat.2004.07.003
12. S. M. Sathe, Suparna Banerjee, Sunil Kumar, and D. N. Sah, Oxide morphology and hydride distribution in irradiated zircaloy-2 pressure tube, *Transactions of the Indian Institute of Metals*, **57**, 631 (2004).
13. Mars G Fontana, High Temperature Corrosion, *Corrosion Engineering*, *3rd Int. ed.*, p. 505, McGraw-Hill Book Company, Singapore (1987).
14. B. Cox, *Journal of Nuclear Materials*, **27**, 1, 1968; **29**, 50-66, 638 (1969).
15. V. F. Urbanic, B. Cox, and G. J. Field, Long Term Corrosion and Deuterium Uptake in CANDU PHWR Pressure Tubes, ASTM STP-939, pp. 189-205, Zirconium in Nuclear Industry (1987).
16. K. Park and D. R. Olander, Oxygen Diffusion in Single –

Crystal Tetragonal Zirconia, *Journal of the Electrochemical Society*, **138**, 1154 (1991). https://iopscience.iop.org/article/10.1149/1.2085733/pdf

17. F. Long, L. Balogh, D. W. Braown, P. Mosbrucker, T. Skippon, C. D. Judge, and M. R. Daymond, Effect of neutron on deformation mechanisms operating during tensile testing of Zr-2.5Nb, *Acta Materialia*, **102**, 352 (2016). https://doi.org/10.1016/j.actamat.2015.09.032